Arch. Metall. Mater. **68** (2023), 2, 499-505

DOI: https://doi.org/10.24425/amm.2023.142428

A. ŞIK[1], A. ÖZER[2*]

THE EFFECTS OF FRICTION STIR WELDING PARAMETERS ON MICROSTRUCTURE, FATIGUE LIFE AND TENSILE PROPERTIES OF ALUMINUM 2024-T3 ALLOY

In this study, Al 2024-T3 alloy plates were joined by using friction stir welding. Welding was performed at a rotational speed of 930, 1450, 2280 rpm and a welding feed rate of 180 mm min^{-1}. The welded samples were analyzed at the microstructural level. Moreover, both bending fatigue tests and tensile tests were performed on samples. At the end of the microstructural examination of the samples welded at the rotational speed of 930 rpm and the welding feed rate of 180 mm min^{-1}, the formation of tunnel defects was observed. The highest fatigue life was obtained at 2280 rpm and 180 mm min^{-1}. The lowest fatigue life was obtained at 930 rpm and 180 mm min^{-1}. The highest ultimate tensile stress was obtained at 2280 rpm/180 mm min^{-1} sample, which shows about a 12% reduction relative to the base material. The lowest ultimate tensile stress was obtained at 930 rpm/180 mm min^{-1} sample. The ultimate tensile stress value of the 930 rpm/180 mm min^{-1} sample decreased by approximately 25%.

Keywords: friction stir welding; microstructure; fatigue life; tensile properties; Al 2024-T3

1. Introduction

In recent years, lightweight materials are preferred instead of heavy structural materials for various engineering applications. Aluminum (Al) and Al alloys, as the most popular non-ferrous metallic materials in the world, are used extensively in different industries like automotive, aerospace and marine due to their low density, resistance to atmospheric corrosion and easy manufacturability [1,2].

In different industries, Al and Al alloys are joined using different welding techniques. However, it is difficult to weld Al alloy components by using conventional welding techniques and these techniques presents great challenges. Conventional fusion welding techniques used for joining Al alloys are prone to creating defects in weld seams such as oxidation, distortion, porosity and cracks. The solid state joining techniques offers a better solution for joining these alloys [3-6].

The 2XXX series Al alloys exhibit precipitation hardening. The hardness and strength of this Al alloy series are significantly higher. However, it is difficult to weld high strength Al alloys such as Al 2024 by conventional fusion welding method due to hot cracking. Therefore, the 2xxx series Al alloys exhibit limited weldability. The dendritic and eutectic structure formed in the fusion zone with conventional fusion welding causes a significant decrease in mechanical behavior [7-10].

For this reason, different welding techniques are required to prevent or reduce welding defects for materials with poor fusion welding capability. Friction stir welding (FSW) is one of these techniques. FSW, which has been developed since the 1990s and is a solid-state welding method, gives positive results in joining Al alloys that are difficult or impossible to join with known fusion welds and especially subjected to age hardening. This method is developed by The Welding Institute (TWI) for joining aluminum alloys [11-18].

The welding process occurs based on the principle of heat formation in the weld zone of the materials to be welded with the rotating tip of the friction tool made of a material harder than the part to be joined (Fig. 1). When the pin enters into the weld zone, the shoulder part made circular movements by touching the surfaces to be joined first. The penetration depth of this tip into the parts to be joined can also be expressed as welding penetration. In addition to the heat generated in the weld zone when the shoulder part of the tool contacts with the material, a truncated cone-like end of the pin is immersed into the softened joining area. A wide area forms in the region that narrows towards the edge of the metal in this softened thermal area but displays friction with shoulder part of the tool (Fig. 1) [19-23].

[1] GAZI UNIVERSITY, FACULTY OF ARCHITECTURE, DEPARTMENT OF INDUSTRIAL DESIGN, 06570 MALTEPE, ANKARA, TURKEY
[2] GAZI UNIVERSITY, TECHNICAL SCIENCES VOCATIONAL SCHOOL, 06374 OSTIM, YENIMAHALLE, ANKARA, TURKEY

* Corresponding author: aozer@gazi.edu.tr

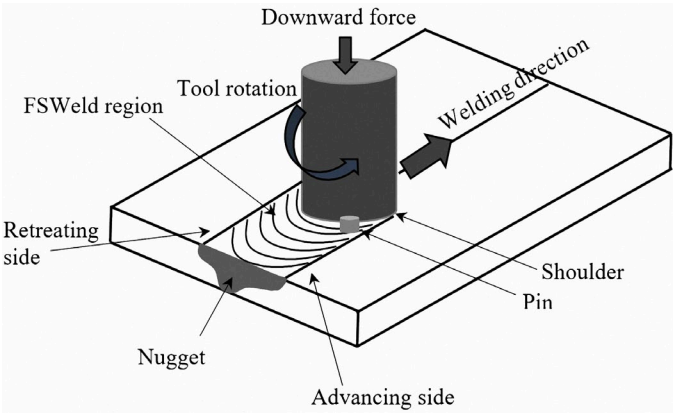

Fig. 1. Schematic illustration of the FSW process

This technique has made it easy to join many products for which it is very difficult to perform a good weld without any gap, crack or a distortion in the part with welding. FSW is considered as an alternative to fusion welding techniques because of its low power requirements, lack of gas shielding and no need for special welding groove preparation. FSW aluminum alloys have been used in aerospace, shipbuilding, automotive, railway, defense industries and have attracted great research interest due to their importance in engineering. This process is used to join metals without fusion and/or filler metal. FSW has many advantages compared to fusion welding techniques of aluminum. Problems caused by fusion welding of aluminum alloys such as the fracture of solidification and liquid cracking are eliminated with FSW due to the solid-state welding technique [7,16,24-29].

Three different areas are observed in the weld zone of materials joined with FSW. These areas are welding nugget zone (NZ), thermo-mechanically affected zone (TMAZ) and external heat affected zone. The NZ microstructure is generally composed of fine and equaxial grains. It has been stated in the literature that the NZ microstructure is formed by continuous dynamic recrystallization and leads to an increase in mechanical properties [7,30-32].

The number of studies conducted on weldability of Al 2024 alloy by using FSW method has increased in recent years. Dressler et al. [33] reported that TiAl6V4 alloy and Al 2024-T3 alloy were successfully combined with friction stir welding. They mentioned the presence of fine recrystallized aluminum alloy grains in the NZ. It was stated that the ultimate tensile strength of the joint reached 73% of AA2024-T3 the base material strength. Cavaliere et al. [7] examined the mechanical and microstructural properties of 2024 and 7075 aluminum alloys joined with FSW. The authors noted that even though the fatigue test results were lower than the base metal, samples joined with FSW gave satisfactory results. Wang et al. [34] examined the fatigue and corrosion properties of Al 2024 alloy plates joined with FSW. The authors reported a dramatic decrease in the fatigue life of samples combined with FSW. Sharifitabar and Nami [35] were studied the FSW weldability of 2024-T4 alloy and Al/Mg_2Si metal matrix cast composites. They stated that while there were no defects such as voids and tunnel deffect in sample welded in one pass, these deffects occur in the stir zone as a result of FSW operations performed with two passes [35].

In this study, Al 2024-T3 alloy plates were joined by using FSW process and the effects of the selected experiment parameters on microstructural properties, fatigue life and tensile properties of the welded joints were examined.

2. Experimental Method

2.1. Material

In this study, Al 2024-T3 alloy, which attracts attention with its properties such as successful microstructure-mechanical property relationship, good machinability, high corrosion resistance, was selected as the test material. Chemical composition, mechanical and physical properties of Al 2024-T3 test material were given in TABLE 1. For the FSS welding process, Al-2024-T3 material with a rectangular cross section of 160×500 mm and a thickness of 4.5 mm was prepared.

2.2. Welding Application

The tool (shoulder and pin) used in friction stir welding equipment was produced of hot work tool steel having AISI H13 (EN X40CrMoV51) standard according to the dimensions

TABLE 1

Chemical composition, mechanical and physical properties of Al 2024 alloy

Chemical composition, %							
Fe	Si	Cu	Mn	Mg	Zn	Ti	Cr
<0.50	<0.50	3.80-4.90	0.30-0.90	1.20-1.80	<0.25	<0.20	<0.10
Mechanical properties							
Heat treatment		Yield strength (MPa)	Tensile strength (MPa)		Elongation (%)		Hardness (HB)
T3		≈345	≈485		≈15		≈125
Physical properties							
Density (gr/cm^3)		Modulus of elasticity (MPa)	Thermal Conductivity (W/mK)		Coefficient of thermal expansion (20-100°C) (1/K)		Electrical Resistance (20°C) (Ohm.cm)
2.78		73100	121		23.2×10^{-6}		5.82×10^{-6}

given in Fig. 2. The diameter of shoulder size was 20 mm. The full length of the tool (shoulder and pin) was 100 mm and the pin height was 4.3 mm. The tool had an M4×0,7 cylindrical pin.

Welding processes were conducted using a semi-automatic milling machine. The edges of the Al 2024 sheets were fixed mechanical clamps to the tabletop part of the milling machine by making face-to-face contact. FSW tool (shoulder and pin) made of AISI H13 tool steel was attached to the vertical spindle axis of the milling machine and FSW process was carried out in this setup. FSW was performed at the constant shoulder plunge depth of 0.2 mm. FSW process parameters and the sample illustrations are given in TABLE 2.

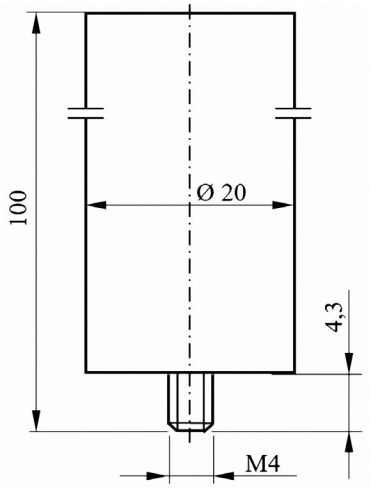

Fig. 2. Dimensions of the pin used in FSW

TABLE 2

Variables used in the FSW process

Specimen notation	Rotational speed (rpm)	Welding Feed Rate (mm min^{-1})
930-180	930	180
1450-180	1450	180
2280-180	2280	180

The sheets joined by friction stir welding method were visually examined to determine possible surface defects before welding. This examination was based on the ANSI/AWS D9.1-90 sheet metal welding code. After making the joints, the experimental samples were subjected to cooling under normal cooling conditions as stated in the relevant standards.

2.3. Microstructure studies and mechanical tests

Microstructural properties, fatigue behaviors and tensile properties of the FSW samples were determined by using metallographic examination and mechanical tests. For this purpose, the samples were cross-sectioned perpendicular to the welding direction and prepared for metallographic inspection, and then etched with a Keller's reagent. Optical microscopy was used to examine the microstructure. The FSW samples were prepared according to DIN 50142 and ASTM E8: 2016 standards for bending fatigue tests and tensile tests, respectively Fig. 3. Eight experimental samples used in this study were made for each welding variable in accordance with the properties of bending fatigue test machine and from non-welded base material in standard sizes. The dimensions of the samples used are given in Fig. 3a for the non-welded base material and in Fig. 3b for the welded samples. Wöhler curves were formed graphically with the data obtained in the experiments. The number of cycles corresponding to the highest value in these curves was obtained by marking logarithmically. In the bending fatigue tests, the value of $N = 2 \times 10^6$ used in scientific studies was applied as the limit cycle number (life). Fig. 3c shows the shape and dimensions of the samples to be subjected to the tensile test.

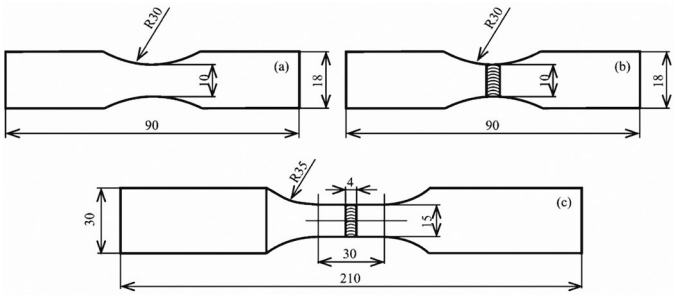

Fig. 3. The samples prepared according to DIN 50142 and ASTM E8: 2016; a) Fatigue test sample of the base material, b) Fatigue test sample of the FSW, c) tensile test sample of the FSW

3. Results and Discussions

3.1. Microstructure Experiment Results

Optical microstructure photograph of Al 2024-T3 alloy are given in Fig. 4. When the micrograph was examined, fine homogeneously dispersed small precipitates (shown with white arrow), precipitate colonies (shown with black arrow) and white fine homogeneously distributed precipitates were observed in the microstructure. It is stated in the literature that black precipitate colonies with homogeneous distribution throughout the microstructure and black fine-dispersed precipitates are intermetallic compounds with the chemical formula $CuAl_2$. Also,

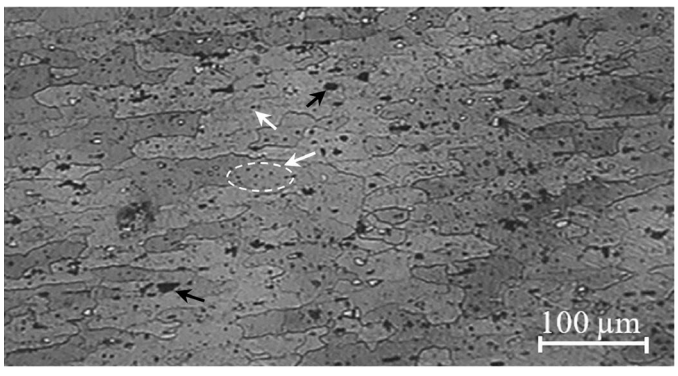

Fig. 4. Microstructure of Al 2024-T3 alloy

according to the literature, it can be said that the fine-white and homogeneously distributed precipitates in the microstructure are intermetallic compounds containing Cu, Mg and elemental Al. The general microstructure (α-phase) consists of aluminum phase grains in FCC crystal structure rich in Cu and other alloying elements [36-41].

Fig. 5 shows microstructure images of the FSW samples joined with different rotational speeds (R_s) at constant 180 mm min^{-1} welding feed rate (W_f) (welding speed). A tunnel defect was detected on sample 930/180 (Fig. 5a). The reasons for the formation of tunnel defect involved heat input, stirring tool design, pin design, and the imbalance in the ratio of R_s to W_f and therefore the lack of sufficient plastic deformation [16,42-45]. In this study, all parameters were kept constant except for R_s. Therefore, it could be asserted that the reason for the formation of the tunnel defect observed in sample 930/180 was the mismatch of the R_s/W_f [16]. In addition, when Fig. 5a is examined, the presence of micro pores in all FSW samples was determined. However, it has been determined that the amount and size of micro pores in the microstructure decrease with increasing R_s.

Micrographs of the 1450/180 and 2280/180 samples given in Fig. 5b shows that the grain coarsening occurred in the TMAZ of the 2280/180 sample. Increasing grain size with increasing R_s is associated with the heat input during FSW. The equation of heat input is as follows [46,47].

$$Q = (4/3)\ \pi^2 \mu R_s P r^3 \quad (1)$$

Q is the heat input (W), μ is the friction coefficient, R_s is the rotational speed (rev s^{-1}), P is the vertical pressure (Pa), and r is the radius of tool shoulder (mm) in this equation. According to the equation, heat input (Q) in FSW depends on R_s. When the W_f and all other parameters were kept constant, increasing R_s had an increasing impact on heat input. Therefore, increasing R_s led to an increase in frictional heat on the welded joint [16,48-50].

Fig. 5b shows the deformation bands was formed in the NZ of the 930/180 sample. During the FSW, the material extruded (compressing by directing) as a result of high temperature and rotation in welding center was exposed to a high deformation in this zone. With the effect of this excessive deformation and high temperature, the grain structures are directed by flattening.

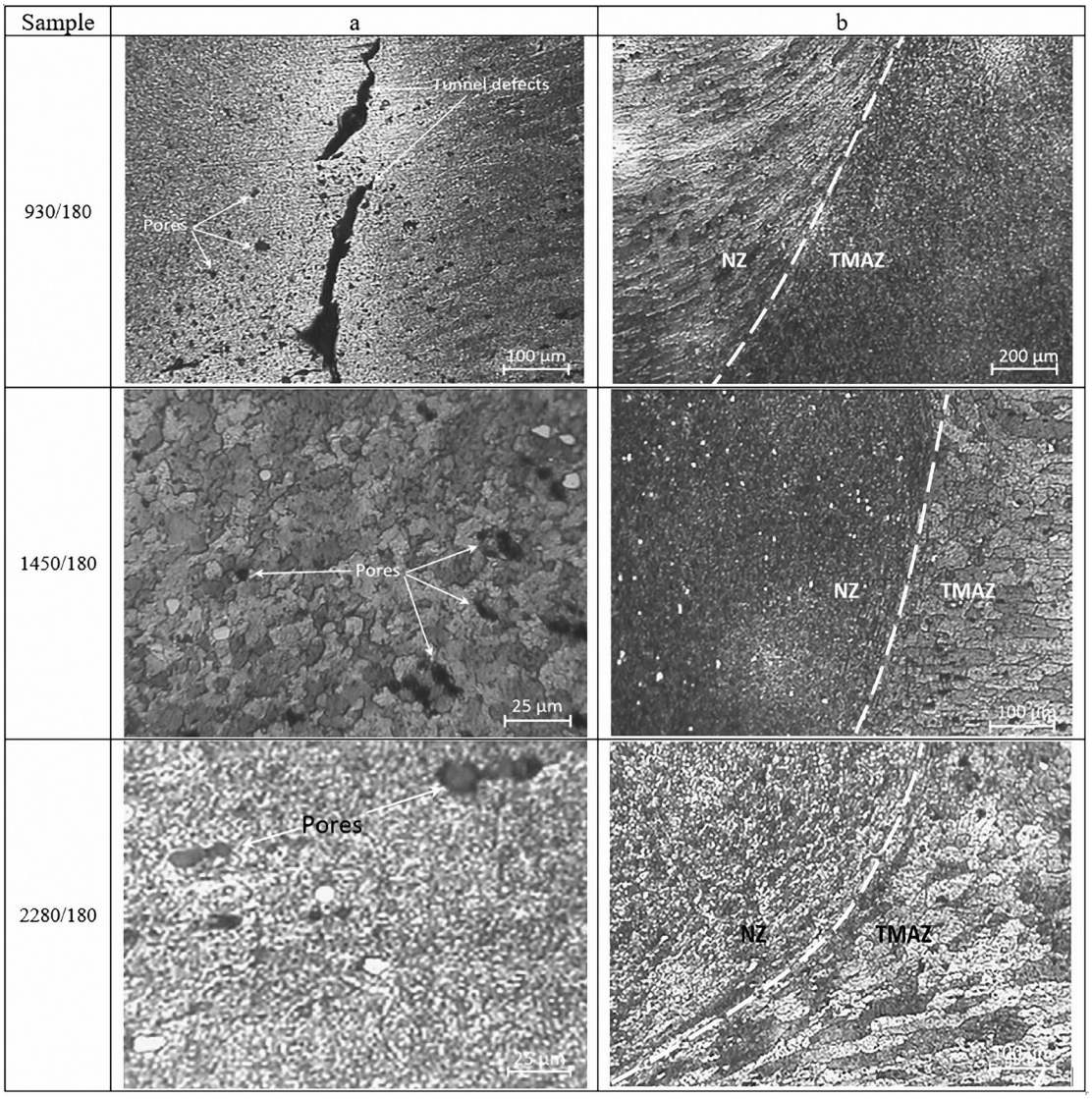

Fig. 5. Micrographs of FSW samples, (a) (NZ), (b) NZ and TMAZ

These directed grain groups caused the formation of deformation bands in NZ. When the microstructure photographs of 1450/180 and 2280/180 samples given in Fig. 5a-b were examined, it was determined that a fine grain structure was occured in NZ by dynamic recrystallization compared to the TMAZ.

3.2. Bending Fatigue Tests

Fig. 6 shows the images of bending fatigue test samples after fracture. Images of a) the fracture form of the bending fatigue test sample obtained from the base material, b) fracture form of the bending fatigue test sample obtained from the welded material, c) a close view of the fracture area and d) the fracture sample were given here. No fracture occurred in the welding seam as shown in Fig. 6b. This confirms that welding process which did not fracture in this zone was robust and carried out in accordance with the standards.-

Fig. 7 shows the bending fatigue test results of the base materials and samples joined by using FSW. As expected, the highest fatigue life values were obtained in the base material. In the joined test samples with FSW, the highest fatigue life was obtained at 2280 rpm and 180 mm min^{-1}; whereas, the lowest fatigue life was obtained at 930 rpm and 180 mm min^{-1}. As can be seen in Fig. 7, the lowest fatigue life values were observed in the sample 930/180. In the sample 930/180, the formation of tunnel defect occurred as a result of the imbalance in R_s/W_f ratio. Tunnel defect produced a notch effect, thus resulted in the lowest fatigue life. When the R_s was increased from 930 rpm to 2280 rpm at constant W_f, the bending fatigue life of the test samples were high. The reason for high bending fatigue life with increasing R_s was the elevated heat generated in the weld zone with the increase of the R_s. Therefore, enough heat would be generated during the welding and the plastic deformation will occur at the desired level. As the R_s increased, the fatigue life values of the samples increased. This is because of the increase of heat generated in the material at high R_s, and so the joints cooled down more slowly. When Fig. 7 is examined, it is seen that the 2280/180 sample has a satisfactory fatigue life.

3.3. Tensile Tests

Fig. 8 shows the tensile test results of the base material and samples joined using the FSW. The base material was given the highest ultimate tensile stress values and elongations (%). In the joined test samples with FSW, the highest ultimate tensile stress was obtained at 2280/180 sample; whereas, the lowest ultimate tensile stress was obtained at 930/180 sample. This tensile test results obtained are consistent with the bending fatigue test results. The tunnel defect occurred in the 930/180 sample and the coarse micropores in its microstructure caused the notch effect (Fig. 5). The ultimate tensile stress value of the 930/180 sample is the lowest due to this effect. Comparing with the ultimate tensile stress value of the base material, the ultimate tensile stress value of the 930/180 sample decreased by approximately 25%. Ultimate tensile stress values have been also significantly affected by R_s, as R_s significantly affects the heat input generated in the joint zone and thus the microstructure. When the R_s was increased from 930 rpm to 2280 rpm at constant W_f, the ultimate tensile stress of the test samples was high. The reason for ultimate tensile stress with increasing R_s was the increased heat generating in the weld zone with the increase of the R_s and thus enough heat would be generated. Increasing heat input caused more homogeneous plastic deformation in the weld area. As a result , both tunnel defect formation was prevented and the size and amount of pores seen decreased. The ultimate tensile

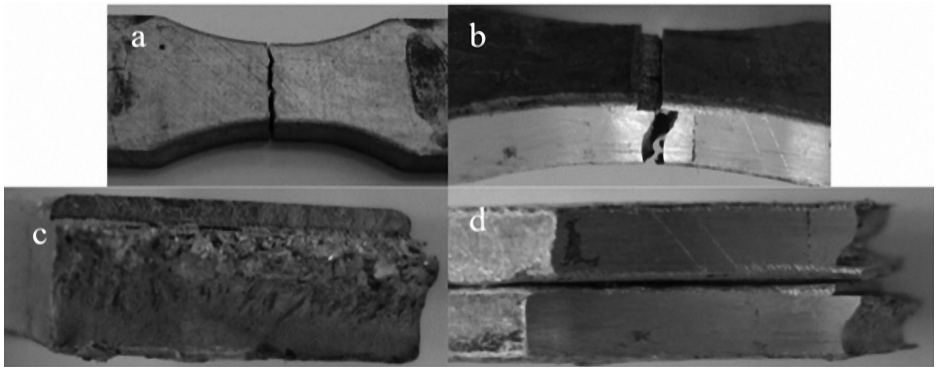

Fig. 6. Images of the fracture samples a) base material, b) welded material, c and d) broken surface

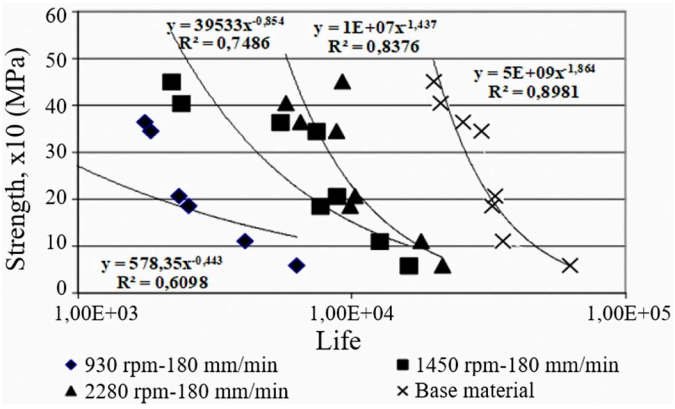

Fig. 7. Bending fatigue test results of the samples

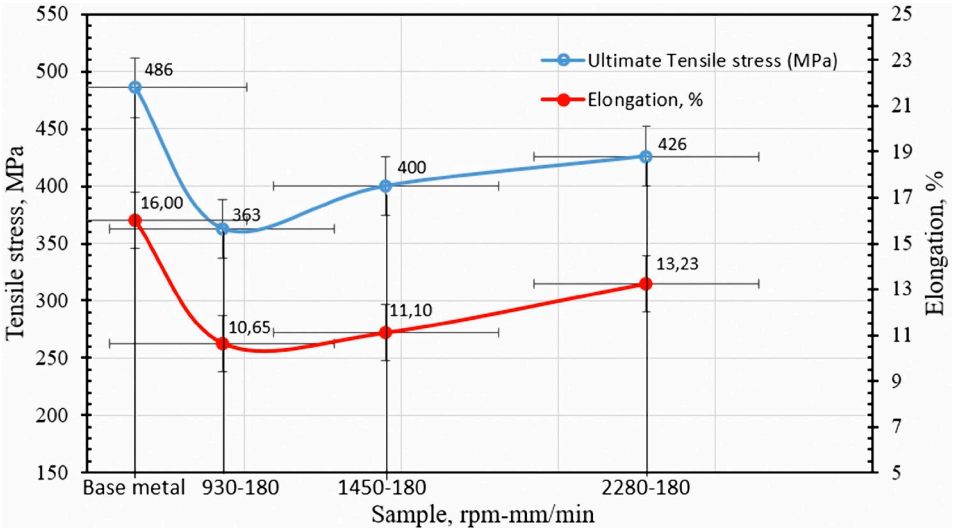

Fig. 8. Tensile test results of the samples

stress value of the 2280/180 sample was 426 MPa, about a 12% reduction relative to the base material was determined.

When the elongation % values given in Fig. 8 were examined, a trend similar to the ultimate tensile stress values were observed. 930/180 sample had given the lowest elongation % value due to tunnel error and micropores occurring in N.Z (Fig. 5). A decrease of approximately 33% was determined in the elongation % value of the 930/180 sample compared to the base metal. Similar to the ultimate tensile stress values, the elongation % values of FSW samples increased with the increasing *Rs*. In response to increasing tensile stress values, a decrease in the elongation % values of FSW specimens can be expected. However, NZ, which contains more homogeneous microstructure and less micropores with increasing *Rs*, caused an increase in elongation % values. The elongation % value obtained in the 2280/180 sample is approximately 17% less than the elongation of the base metal. It is approximately 24% higher than the elongation of the 930/180 sample.

4. Conclusions

The main conclusions of this study are summarized below;

1. A tunnel defect was detected on sample 930 rpm/180 mm min^{-1}.
2. It was observed that the grain coarsening occurred in the TMAZ.
3. Deformation bands were formed in NZ due to excessive deformation at a low R_s/W_s ratio. (930 rpm/180 mm min^{-1}). Fine grain structure was formed in NZ by recrystallization with increasing *Rs*.
4. The highest fatigue life values were obtained in the base material. In the joined test samples with FSW, the highest fatigue life was obtained at 2280 rpm/180 mm min^{-1}. The lowest fatigue life was obtained at 930 rpm/180 mm min^{-1}.
5. In the joined test samples with FSW, the highest ultimate tensile stress was obtained at 2280 rpm/180 mm min^{-1} sample, about a 12% reduction relative to the base material. The lowest ultimate tensile stress was obtained at 930 rpm/180 mm min^{-1} sample. The ultimate tensile stress value of the 930 rpm/180 mm min^{-1} sample decreased by approximately 25%. The elongation obtained in the 2280 rpm/180 mm min^{-1} sample is approximately 17% less than the elongation of the base metal. A decrease of approximately 33% was determined in the elongation value of the 930 rpm/180 mm min^{-1} sample compared to the base metal.

Acknowledgements

The fatigue strength tests of this study were supported by Gazi University Scientific Research Projects Office (Project code 48/2017-01).

REFERENCES

[1] M. Karthikeyan, Jonah, Mater. Res. Express. **8** (2), 026502 (2021). DOI: https://doi.org/10.1088/2053-1591/abde57

[2] F. Ortega, W. Fernández, J.F. Santa, J. Unfried-Silgado, Journal of Mechanical Engineering And Sciences (JMES) **14** (4), 7507-7519 (2020). DOI: https://doi.org/10.15282/jmes.14.4.2020.17.0591-2020

[3] K. Fuse, V. Badheka, Metals. **11** (1), 16 (2021) DOI: https://doi.org/10.3390/met11010016

[4] L. Zhou, G.H. Li, C.L. Liu, J. Wang, Y.X. Huang, J.C. Feng, F.X. Meng, Int. J. Adv. Manuf. Technol. **89**, 3509-3516 (2017). DOI: https://doi.org/10.1007/S00170-016-9318-5

[5] A. Cisko, J. Jordon, R. Amaro, P. Allison, J. Wlodarski, Z. McClelland, L. Garcia, T.A. Rushing, Mat. Manuf. Process. **35** (10), 1-8 (2020). DOI: https://doi.org/10.1080/10426914.2020.1765249

[6] B. Gungor, E. Kaluc, E. Taban, A. Sik, Materials and Design. **56**, 84-90 (2014). DOI: https://doi.org/10.1016/j.matdes.2013.10.090

[7] P. Cavaliere, R. Nobile, F.W. Panella, A. Squillace, Int. J. Mach. Tool. Manu. **46** (6), 588-594 (2006). DOI: https://doi.org/10.1016/j.ijmachtools.2005.07.010

[8] J.Q. Su, T.W. Nelson, R. Mishra, M. Mahoney, Acta Materialia. **51** (3), 713-729 (2003). DOI: https://doi.org/10.1016/S1359-6454(02)00449-4

[9] C.G. Rhodes, M.W. Mahoney, W.H. Bingel, Scripta Mater. **36** (1), 69-75 (1997). DOI: https://doi.org/10.1016/S1359-6462(96)00344-2

[10] V. Dixit, R.S. Mishra, R.J. Lederich, R. Talwar, Sci. Technol. Weld. Joi. **12** (4), 334-340 (2007). DOI: https://doi.org/10.1179/174329307X197593

[11] R. Nandan, T. DebRoy, H.K.D.H. Bhadeshia, Prog. Mater. Sci. **53** (6), 980-1023 (2008). DOI: https://doi.org/10.1016/j.pmatsci.2008.05.001

[12] M.K. Sued, D. Pons, J. Lavroff, E.H. Wong, Materials and Design. **54**, 632-643 (2014). DOI: https://doi.org/10.1016/j.matdes.2013.08.057

[13] M. Boz, A. Kurt, Materials and Design. **25** (4), 343-347 (2004), DOI: https://doi.org/10.1016/j.matdes.2003.11.005

[14] A. Kurt, M. Boz, M. Özdemir, J. Fac. Eng. Arch. Gazi Univ. **19** (2), 191-197 (2004).

[15] A. Ozer, A. Sik, B. Cevik, M. Ozer, Kovove Mater. **55**, 107-114 (2017). DOI: https://doi.org/10.4149/km_2017_2_107

[16] Z. Barlas, H. Uzun, Journal of Achievements in Materials and Manufacturing Engineering. **30** (2), 182-186 (2008).

[17] L.E. Murr, G. Liu, J.C. McClure, J. Mater. Sci. **33**, 1243-1251 (1998).

[18] Ay. ŞIK, Journal of Polytechnic. **9** (2), 125-130 (2006).

[19] A. Yuruk, B. Cevik, N. Kahraman, Mater. Test. **61** (10), 941-946 (2019). DOI: https://doi.org/10.3139/120.111404

[20] C.J. Dawes, W.M. Thomas, Weld. J. **75**, 41-45 (1996).

[21] R.R. Varma, A. Bin Ibrahim, Mohammed, A. Bin Mansor, International Journal of Mechanical and Production Engineering **2** (5), 1-5 (2014).

[22] M. Mijajlovic, D. Milcic, V.N. Stanojevic, M. Milcic, Ser. A: Appl. Math. Inform. and Mech. **4** (2), 65-70 (2012).

[23] P. Cavaliere, G. Campanile, F. Panella, A. Squillace, J. Mater. Process. Tech. **180** (1-3), 263-270 (2006). DOI: https://doi.org/10.1016/j.jmatprotec.2006.06.015

[24] B. Cevik, Y. Ozcatalbas, B. Gulenc, Kovove Mater. **54** (4), 241-247 (2016). DOI: https://doi.org/10.4149/km_2016_4_241

[25] B. Cevik, Y. Ozcatalbas, G. Gulenc, Prakt. Metallogr-Pr M. **53** (1), 6-23 (2016). DOI: https://doi.org/10.3139/147.110363

[26] A. Chandrashekar, H.N. Reddappa, B.S. Ajaykumar, Mater. Today-Proc. **2** (4-5), 3491-3500 (2015). DOI: https://doi.org/10.1016/j.matpr.2015.07.325

[27] H.B. Chen, K. Yan, T. Lin, S.B. Chen, C.Y. Jiang, Y. Zhao, Mat. Sci. Eng. A-Struct. **433** (1-2) (2006). DOI: https://doi.org/10.1016/j.msea.2006.06.056

[28] A. Rahimzadeh, A. Heidarzadeh, A. Mohammadzadeh, G. Moeini, J. Mater. Res. Technol. **9** (5), 11154-11161(2020). DOI: https://doi.org/10.1016/j.jmrt.2020.08.010

[29] I. Charit, R.S. Mishra, M. Mahoney, Scripta Mater. **47** (9), 631-636 (2002). DOI: https://doi.org/10.1016/S1359-6462(02)00257-9

[30] C.G. Rhodes, M.W. Mahoney, W.H. Bingel, M. Calabrese, Scripta Mater. **48** (10), 1451-1455 (2003). DOI: https://doi.org/10.1016/S1359-6462(03)00082-4

[31] K.V. Jata, S.L. Semiatin, Scripta Mater. **43** (8), 743-749 (2000). DOI: https://doi.org/10.1016/S1359-6462(00)00480-2

[32] U. Dressler, G. Biallas, U.A. Mercado, Mat. Sci. Eng. A-Struct. **526** (1-2), 113-117 (2009). DOI: https://doi.org/10.1016/j.msea.2009.07.006

[33] L. Wang, L. Hui, S. Zhou, L. Xu, B. He, T. Nonferr. Metal. Soc. **26** (11), 2830-2837 (2016). DOI: https://doi.org/10.1016/S1003-6326(16)64411-4

[34] M. Sharifitabar, H. Nami, Compos. Part. B-Eng. **42** (7), 2004-2012 (2011). DOI: https://doi.org/10.1016/j.compositesb.2011.05.025

[35] Z. Huda, N.I. Taib, T. Zaharinie, Mater. Chem. Phys. **113** (2-3), 515-517 (2009). DOI: https://doi.org/10.1016/j.matchemphys.2008.09.050

[36] İ. Karaağaç, M.O. Kabakçi, M.Y. Demirel, GU J. Sci. Part C. **8** (1) 169-181 (2020).

[37] J. Zhou, S. Xu, S. Huang, X. Meng, J. Sheng, H. Zhang, J. Li, Y. Sun, E. A. Boateng, Metals **6**, 279 (2016). DOI: https://doi.org/10.3390/met6110279

[38] M.L. Siqueiraa, A. da Silva, M. de Lourdes N.M. Melo, G. Rodrigues, Mat. Res. **22** (4), (2019). DOI: https://doi.org/10.1590/1980-5373-mr-2018-0598

[39] A.E. Hughes, R. Parvizi, M. Forsyth, Corros. Rev. **33** (1-2), 1-30 (2015). DOI: https://doi.org/10.1515/corrrev-2014-0039

[40] J.A. DeRose, A. Bałkowiec, J. Michalski, T. Suter, K.J. Kurzydlowski, P. Schmutz, WIT Transactions on State of the Art in Science and Engineering. **61**, 23-38 (2012). DOI: https://doi.org/10.2495/978-1-84564-752-0/003

[41] A. Şık, M. Önder, Kovove Mater. **50** (2), 131-137 (2012). DOI: https://doi.org/10.4149/km_2012_2_131

[42] M. Erdem, Int. J. Adv. Manuf. Technol. **76**, 1583-1592 (2015). DOI: https://doi.org/10.1007/s00170-014-6387-1

[43] G. Çam, S. Mistikoglu, M. Pakdil, Welding Journal **88** (11), 225-232 (2009).

[44] M.W. Mahoney, C.G. Rhodes, J.G. Flintoff, R.A. Spurling, W.H. Bingel, Metall. Mater. Trans. A. **29**, 1955-1964 (1998). DOI: https://doi.org/10.1007/s11661-998-0021-5

[45] M.S. Moghaddam, R. Parvizi, M. Haddad-Sabzevar, A. Davoodi, Materials and Design. **32** (5), 2749-2755 (2011). DOI: https://doi.org/10.1016/j.matdes.2011.01.015

[46] H.S. Park, T. Kimura, T. Murakamic, Y. Nagano, K. Nakata, M. Ushio, Mat. Sci. Eng. A-Struct. **371** (1-2), 160-169 (2004). DOI: https://doi.org/10.1016/j.msea.2003.11.030

[47] I. Uygur, Arch. Metall. Mater. **57** (1), 53-60 (2012). DOI: https://doi.org/10.2478/v10172-011-0152-3

[48] A. Heidarzadeh, T. Saeid, T, Materials and Design. **52**, 1077-1087 (2013). DOI: https://doi.org/10.1016/j.mates.2013.06.068

[49] A. Heidarzadeh, M. Jabbari, M. Esmaily, Int. J. Adv. Manuf. Technol. **77**, 1819-1829 (2015). DOI: https://doi.org/10.1007/s00170-014-6543-7

[50] H. Farrokhi, A. Heidarzadeh, T. Saeid, Sci. Technol. Weld. Join. **18** (8), 697-702 (2013). DOI: https://doi.org/10.1179/1362171813Y.0000000148